

# Single-step implementation of high fidelity $n$ -bit Toffoli gates

S. E. Rasmussen<sup>1,\*</sup> and N. T. Zinner<sup>1,2,†</sup>

<sup>1</sup>*Department of Physics and Astronomy, Aarhus University, DK-8000 Aarhus C, Denmark*

<sup>2</sup>*Aarhus Institute of Advanced Studies, Aarhus University, DK-8000 Aarhus C, Denmark*

(Dated: December 21, 2024)

The family of  $n$ -bit Toffoli gates, with the 2-bit Toffoli gate as the figurehead, are of great interest in quantum information as they can be used as universal gates and in quantum error correction, among other things. Here we present a simple single-step implementation of arbitrary  $n$ -bit Toffoli gates. The gate time of the implementation is independent of the number of control qubits, and the fidelities of our systems are well above 0.98 for up to five control qubits, with the major contribution to error coming from the qubit decoherence time. We discuss an implementation of the gates using superconducting circuits, however, the ideas presented in this paper is not limited to such implementation. We also show how these ideas can be used to make a series of CNOT-gates more efficient by performing all CNOT-gates in a single time step. Lastly we combine all of the above to create efficient quantum error correction codes. Specifically we simulate the three-qubit bit flip code and the Steane seven-qubit encoding, both with high fidelity.

## I. INTRODUCTION

The  $n$ -bit Toffoli gates are a family reversible logic gates, where each gate have  $n$  control bits and one bit which is inverted if the control bits are in the right state. The  $n$ -bit Toffoli gates, and especially the 2-bit Toffoli gate, simply known as *the* Toffoli gate [1], are of great interest in the field of quantum information [2]. The 2-bit Toffoli gate, on its own, is a universal gate in classical computing and together with the Hadamard gate it constitutes a universal set of quantum gates [2]. The  $n$ -bit Toffoli gates are further important since they play a pivotal role in schemes for quantum error correction [3, 4], fault tolerant quantum computing [5, 6], and in Shor's algorithm [7].

While simple high fidelity implementations of the 1-bit Toffoli gate, simply known as the CNOT-gate, have been achieved within the last decades [8–11], a high-fidelity Toffoli gate with  $n \geq 2$  remains elusive. This is due to the fact that gates operating on three or more qubit systems are difficult to realize and that at least five two-qubit gates and several single-qubit gates are necessary for implementing the 2-bit Toffoli gate without using a three-qubit gate [12, 13]. Most experimental implementations of the Toffoli gate are based on this two-qubit implementation and achieves a rather poor fidelity, using ion trap systems [14], or linear optics [15]. Implementations in superconducting circuits have also been achieved using qudits with more than the two lowest states, again with rather low fidelities [16, 17].

In recent years a lot of effort has been put into creating simpler schemes for the implementation of the 2-bit Toffoli gate using fewer steps [18–20], with experimental implementations reaching fidelities up to approximately 0.98 using single photon post selection techniques [21] and in ultra cold neutral atoms [22].

Implementations of higher order  $n$ -bit Toffoli, (i.e.  $n > 2$ ) gate is relatively unexplored, and these gates are usually based on putting together several lower order gates, much in the same way the 2-bit Toffoli gate can be created with two-qubit gates [23, 24].

Here we present a simple single-step implementation of the  $n$ -bit Toffoli gate for an arbitrary  $n$ . The idea behind the implementation can be realized using different schemes for quantum information processing, and we include circuit design for an implementation of the Toffoli gate in superconducting circuits. The gate is performed in a single step in the sense that it only requires a single drive on the target qubit. This means that the gate time is independent of the number of control qubits. By simulating the gates we find that when decoherence is neglected the fidelity is approximately constant above 0.995 for up to five control qubits, and when decoherence is included the fidelity stays above 0.98. This simple idea can also be used to perform several CNOT-gates in series more effectively, as they can be applied all at once. This opens up for some quite effective error correcting since encoding of the qubits can be done in fewer steps.

The paper is organized as follows: In Sec. II we present a simple Hamiltonian and show how it yields an  $n$ -bit Toffoli gate. We also discuss the effectiveness of the gate exploring the important  $n = 2$  case as an example in Sec. II A. We further, in Sec. II B, present an implementation using superconducting circuits of the 2-bit Toffoli gate and discuss how to expand it to more controls. In Sec. III we explain how to use the same ideas as in Sec. II to implement a CNOT-gate on several qubits at the same time. In Sec. IV we put the two previous ideas together and show an efficient quantum error correction by simulating the three-qubit bit flip correcting code and the Steane seven-qubit code.

---

\* stig@phys.au.dk

† zinner@phys.au.dk

## II. IMPLEMENTATION OF THE $n$ -BIT TOFFOLI GATE

Consider  $n + 1$  qubits each with frequency  $\Omega_i$ . The first  $n$  qubits are connected to the last qubit, denoted with a 0, by an Ising coupling  $J_i^z$ . We drive the zeroth qubit with a field with a time dependent amplitude  $B(t)$ . The Hamiltonian of the system is

$$\hat{H} = \hat{H}_0 + \frac{1}{2} \sum_{i=1}^n J_i^z \sigma_i^z \sigma_0^z + B_0(t) \sigma_0^y, \quad (1)$$

where  $\sigma^{x,y,z}$  denotes the Pauli operators, and the non-interacting part of the Hamiltonian is given as

$$\hat{H}_0 = -\frac{1}{2} \sum_{i=0}^n \Omega_i \sigma_i^z. \quad (2)$$

The amplitude of the driving field is given as

$$B_j(t) = J \cos [(\Omega_j + \omega_j)t], \quad (3)$$

for  $j = 0$  where  $\omega_j = \omega_0$  is thus far an undetermined frequency. Note that we could just as well have used  $\sigma_0^x$  for the driving field. Using Eq. (2) we change into the interacting picture and obtain

$$\begin{aligned} \hat{H}_I = & \frac{1}{2} \sum_{i=1}^n J_i^z \sigma_i^z \sigma_0^z \\ & + \frac{i}{2} J [\sigma_0^+ e^{i\omega_0 t} - \sigma_0^- e^{-i\omega_0 t}], \end{aligned} \quad (4)$$

where we have used the rotating wave approximation and assumed  $|2\Omega_{n+1} + \omega_j| \gg J$ . We change into a frame rotating with the diagonal of the Hamiltonian, which yields

$$\begin{aligned} \hat{H}_{\text{rot}} = & \frac{i}{2} J \left[ \sigma_0^+ e^{i(\omega_j + \sum_{i=1}^n J_i^z \sigma_i^z)t} \right. \\ & \left. - \sigma_0^- e^{-i(\omega_j + \sum_{i=1}^n J_i^z \sigma_i^z)t} \right]. \end{aligned} \quad (5)$$

We now chose  $\omega_0 = \sum_{i=1}^n J_i^z$ , and assume  $J_i^z \gg J$  for all  $i$ , i.e., the Ising interaction is much larger than the driving. Note that we do not require the  $J_i^z$ 's to be equal, but we do require them to be of the same order of magnitude for one of them to not dominate over the others. With these conditions both terms of  $H_{\text{rot}}$  will rotate rapidly, and can thus be neglected using the rotating wave approximation, unless all of the control qubits are in the state  $|1\rangle$ . This means that our Hamiltonian effectively becomes

$$\hat{H}_{\text{rot}} = \frac{i}{2} J |\tilde{1}\rangle \langle \tilde{1}|_C \otimes \sigma_T^y, \quad (6)$$

where subscript  $C$  denotes the state of the control qubits, i.e., the first  $n$  qubits, and  $T$  denotes the state of the target qubit, i.e., the zeroth qubit. The state  $|\tilde{1}\rangle_C = |11\dots 1\rangle_C$  denotes the state where all control qubits are in the state  $|1\rangle$ .

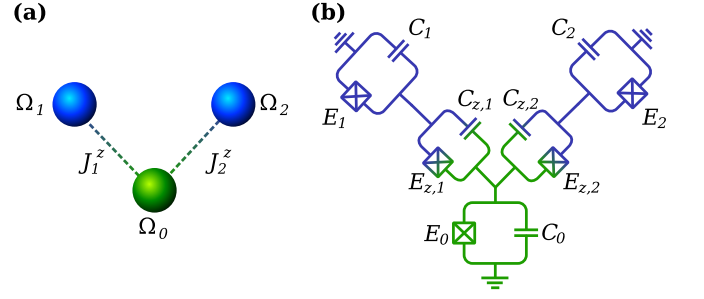


Figure 1. Implementation of the 2-bit Toffoli gate. Figure (a) shows a schematic representation of the model implementing the Toffoli gate, with the green spheres representing the target qubit and the blue spheres representing the control qubits. Figure (b) shows the superconducting circuit yielding the model in figure (a). The different parts of the system are colored according to their role, as per (a).

We can calculate the time evolution operator by taking the matrix exponential,  $\hat{U}(t) = \exp(i\hat{H}_{\text{rot}}t)$ , which yields

$$\begin{aligned} \hat{U}(t) = & \hat{I}_C \otimes \hat{I}_T + \cos\left(\frac{Jt}{2}\right) |\tilde{1}\rangle \langle \tilde{1}|_C \otimes \hat{I}_T \\ & - i \sin\left(\frac{Jt}{2}\right) |\tilde{1}\rangle \langle \tilde{1}|_C \otimes \sigma_T^x, \end{aligned} \quad (7)$$

where  $\hat{I}_C$  denotes the reduced identity of the control qubits where the states  $|\tilde{1}\rangle \langle \tilde{1}|_C$  have been removed. The identity of the target qubit is denoted  $I_T$ , and  $\sigma_T^x = |1\rangle \langle 0| + |0\rangle \langle 1|$  denotes the Pauli X-gate which is equivalent to the NOT-gate.

From Eq. (7) we see that for times  $T = (2m + 1)\pi/J$ ,  $m \in \mathbb{Z}$  the time evolution operator takes the form of an  $n$ -bit Toffoli gate

$$\hat{U}(t = T) = \hat{I}_C \otimes \hat{I}_T \pm i |\tilde{1}\rangle \langle \tilde{1}|_C \otimes \sigma_T^x, \quad (8)$$

with a phase of  $\pm i$  on the target qubit if it is changed, depending on the sign of  $\mp|J|$ . Such a phase can be taken care of with a single-qubit phase gate, an operation which can be done in approximately zero time [25].

### A. Example: The Toffoli gate

In order to illuminate the performance of the system operated as an  $n$ -bit Toffoli gate we explore the example of the 2-bit Toffoli gate. We chose this example due to its merits as mentioned in the introduction. A schematic presentation of the model yielding the Toffoli gate can be seen in Fig. 1(a), which corresponds to Eq. (1) with  $n = 2$  and not including the driving.

We characterize the performance of the Toffoli gate by calculating the average process fidelity, which is defined as [2, 26–28]:

$$\bar{F} = \int d\psi \langle \psi | \hat{U}^\dagger \mathcal{E}(\psi) \hat{U} | \psi \rangle, \quad (9)$$

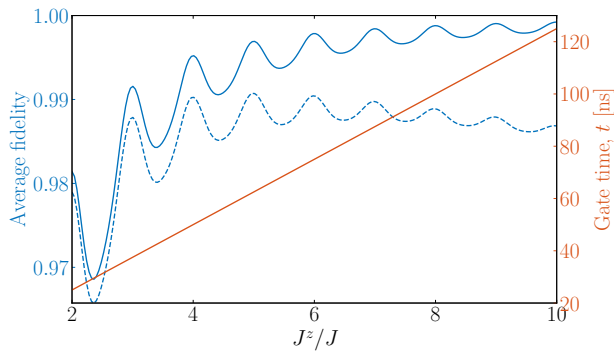


Figure 2. Simulation of the 2-bit Toffoli gate for different values of the driving  $J$ . The blue line indicates the average fidelity, while the red line indicates the gate time  $T$ . The dashed blue line is the average fidelity with a decoherence time of  $T_1 = T_2 = 30 \mu\text{s}$ , while the solid is without decoherence.

where the integration is performed over the subspace of all possible initial states and  $\mathcal{E}$  is the quantum map realized by our system. We simulate the system using the Lindblad Master equation and the interaction Hamiltonian of Eq. (4) using the QuTiP Python toolbox [29]. The result is then transformed into the frame rotating with the diagonal of the Hamiltonian, and then the average fidelity is calculated.

For all simulations we have  $J^z/(2\pi) = 40 \text{ MHz}$ , while we change the driving  $J/(2\pi)$  from 4 to 20 MHz. The average fidelity of the simulation can be seen in Fig. 2 together with the gate time. The figure shows both the average fidelity without any decoherence and with decoherence time of  $T_1 = T_2 = 30 \mu\text{s}$  [30]. Without any decoherence we find that the average fidelity increases asymptotically towards 1 as the driving decreases, with the only expense being an increase in gate time. Since decoherence increases over time, a longer gate time means lower fidelity, which is exactly what we observe when including decoherence in the simulations. In this case we find that the fidelity peaks just above 0.99 at  $J^z/J = 5$ , which yields a gate time of  $T = 62.5 \text{ ns}$ . This fidelity is higher than any previously measured Toffoli gate fidelities [21, 22]. However, we note that the fidelity is dependent on the parameters  $J$  and  $J^z$  thus changing these will change the fidelity. The oscillation of the average fidelity is due to a small mismatch in the phase of the evolved state compared to the desired matrix in Eq. (7), which disappears when  $J^z/J \in \mathbb{Z}$ .

We investigate the peak fidelity of the  $n$ -bit Toffoli gate as a function of the number of control qubits. This is done by simulating the gate for different  $n$  but with  $J^z/J = 5$  in all cases. The result are seen in Fig. 3. Surprisingly we find that when we do not include the decoherence of the qubits the average fidelity is not just constant, it increases when there are more than two control qubits and we stay above 0.995 in fidelity for all cases. The increase in fidelity can be understood since when  $n$  increases,  $\omega$  increases

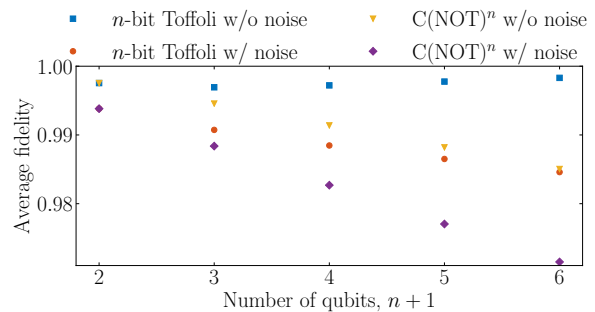


Figure 3. Average fidelity as a function of the number of qubits for the  $n$ -bit Toffoli gate and the  $C(\text{NOT})^n$  gate. Simulations done with noise have a decoherence time of  $T_1 = T_2 = 30 \mu\text{s}$ . All simulations are done with  $J^z/J = 5$ , i.e., peak fidelity cf. Fig. 2.

as well, as it is the sum of all Ising couplings, which means that the approximation yielding Eq. (4) becomes more accurate. When decoherence is included the fidelity decreases as the number of qubits increases as one would expect. Thus we can conclude that the major contribution to error in the scheme is the decoherence of the qubits.

## B. Superconducting circuit implementation

A possible implementation of the 2-bit Toffoli gate using superconducting circuits can be seen in Fig. 1(b). The circuit is inspired by the circuit realizing the coherent quantum router in Ref. [31] The circuit consists of three transmon qubits [32, 33], where two of them are connected to the third by Josephson junctions, with as small a parasitic capacitance as possible. Such a circuit has the following Hamiltonian

$$\hat{H}_{\text{circ}} = \frac{1}{2} \hat{\mathbf{p}}^T K^{-1} \hat{\mathbf{p}} - \sum_{i=0}^n E_i \cos \hat{\varphi}_i - \sum_{i=1}^n E_z \cos(\hat{\varphi}_0 - \hat{\varphi}_i), \quad (10)$$

where  $\hat{\varphi}_i$  are the node fluxes and  $\hat{\mathbf{p}}^T = (\hat{p}_0, \hat{p}_1, \hat{p}_2)$  are the conjugate momenta, fulfilling the commutator relation  $[\hat{\varphi}_i, \hat{p}_j] = i\delta_{ij}$ . The Hamiltonian is the general Hamiltonian for an  $n$ -bit Toffoli gate, and in the case of Fig. 1(b) one needs  $n = 2$ . The capacitive couplings yields transversal  $XX$ -couplings between all the qubits in the model. We are, however, not interested in these couplings, and thus we require  $C_z \ll C_i$ , for  $i = 0, 1, 2, \dots, n$  which will leave the capacitance matrix being approximately diagonal, effectively suppressing undesired transversal  $XX$ -couplings between the control qubits stemming from the capacitances. We further detune the target qubit from the control qubit such that the remaining  $XX$ -couplings is suppressed. This leaves only longitudinal  $ZZ$ -couplings as desired. This limit were the longitudinal coupling domi-

nates over the transversal couplings is within experimental reach [34]. When truncating the Hamiltonian in Eq. (10) to a two level system one reaches the non-driving term of the Hamiltonian in Eq. (4). We obtain the driving part of the Hamiltonian by applying a microwave field to the third qubit, i.e., to the green part of the circuit in Fig. 1. A detailed calculation going from the circuit design to the gate Hamiltonian can be found in Appendix A.

### III. A SINGLE CONTROL, MULTIPLE NOT-GATES

Multiple application of a CNOT-gate on several different qubits, with the same qubit controlling all the gates, are essential in many aspects of quantum information, particularly in error correction such as Shor's code [2]. We therefore present a scheme for implementing multiple CNOT-gates with the same control qubit in a single time step. We will refer to this scheme as a C(NOT)<sup>n</sup>-gate.

Starting with  $n + 1$  qubits, the first  $n$  qubits are connected with Ising couplings to the zeroth qubit as in the  $n$ -bit Toffoli gate. We now drive the first  $n$  qubits instead of the zeroth qubit. Thus the Hamiltonian takes the form

$$\hat{H} = \hat{H}_0 + \frac{1}{2} \sum_{i=1}^n J_i^z \sigma_i^z \sigma_0^z + \sum_{i=1}^n B_i(t) \sigma_i^y, \quad (11)$$

where  $H_0$  is given in Eq. (2) and the amplitude of the driving is given in Eq. (3). This is essentially the system as depicted in Fig. 1(a) but with driving on the blue qubits. Changing into the frame rotating with the diagonal of the Hamiltonian we find

$$\hat{H}_{\text{rot}} = \frac{i}{2} J \sum_{i=1}^n \left[ \sigma_i^+ e^{i(\omega_i + J_i^z \sigma_0^z)t} - \sigma_i^- e^{-i(\omega_i + J_i^z \sigma_0^z)t} \right]. \quad (12)$$

This Hamiltonian flips the spin of the  $n$  target qubits depending on the state of the single control qubit, if we require  $\omega_i = J_i^z$ . This happens at the same time since the single driving and the time evolution operator takes the form

$$\begin{aligned} \hat{U}(t=T) = & |0\rangle\langle 0|_C \otimes \bigotimes_{i=1}^n \hat{I}_{T_i} \\ & + e^{-in\pi/2} |1\rangle\langle 1|_C \otimes \bigotimes_{i=1}^n \sigma_{T_i}^x, \end{aligned} \quad (13)$$

where  $\hat{I}_{T_i}$  is the identity of the  $i$ th target qubit and  $\sigma_{T_i}^x$  is the Pauli X-gate of the  $i$ th target qubit. We find that the phase on the flipping part of the operator is dependent on the number of target qubits. It makes no difference, however, as it can still be taken care of [25].

Since the Hamiltonian is constructed in the same way as the  $n$ -bit Toffoli gate, one can use the same superconducting circuit design for both the  $n$ -bit Toffoli gate and

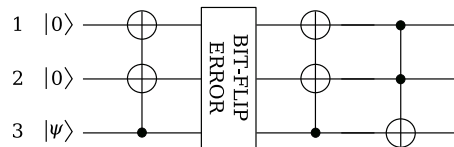


Figure 4. Effective three-qubit error correction code using two C(NOT)<sup>2</sup> gates and a Toffoli gate. We denote the top qubit 1, the middle qubit 2 and the lowest qubit 3.

the C(NOT)<sup>n</sup>-gate. It is simply a matter of which qubits are driven with a microwave field. This also means that a numerical simulation of the C(NOT)<sup>n</sup> gate as a function of the ratio  $J^z/J$  yields an average fidelity comparable to the one for the  $n$ -bit Toffoli gate in Fig. 2, however with a slightly lower fidelity since  $\omega_i$  is now only dependent on one Ising coupling coefficient and not the sum of all of them. This means that the approximation leading to Eq. (4) is not improved by adding more qubits as in the case of the  $n$ -bit Toffoli gate. The peak average fidelity can be seen in Fig. 3, where the average fidelity decreases as a function of the number of qubits. Note that the 1-bit Toffoli gate is the same as the CNOT-gate, which is why the average fidelities are identical in this case.

## IV. APPLICATION OF THE SYSTEM

In this section we discuss how to use the results above to create an efficient error correction code. We consider on the three-qubit bit flip code [2] and the Steane seven-qubit code [35, 36]. We focus on bit flip rather than phase errors in the three qubit code, since the decay time for relaxation is usually half the decay time for dephasing in the case of transmons [33, 37]. One can however easily change the code into correcting phase errors by applying Hadamard gates around the source of error [2].

The three-qubit code has previously been implemented using superconducting circuits to a fidelity of 0.85 [17] and with trapped ions to a fidelity of approximate 0.98 [38]. The Steane seven-qubit code have been implemented with a fidelity between 0.85 and 0.95 using trapped ions [39].

### A. Three-qubit bit flip code

The original three-qubit bit flip code works by first applying two CNOT-gates before the error source, and then two CNOT-gates after the error followed by a single 2-bit Toffoli gate. This means a total of 5 steps. However, using our results the code can be performed in merely three steps: Apply a single C(NOT)<sup>2</sup>-gate before the source of error, a single C(NOT)<sup>2</sup> gate after the error, and finally a single  $n$ -bit Toffoli gate. A quantum circuit of the error correcting code can be seen in Fig. 4.

The error correction code has been simulated using the Lindblad Master equation using the QuTiP Python

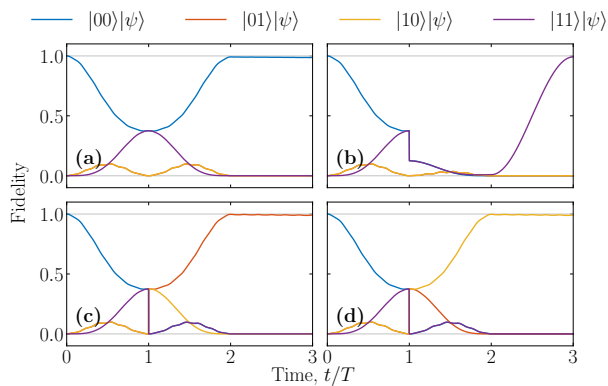


Figure 5. Average fidelity of different states found by simulating the quantum error correction code shown in Fig. 4 using the gates developed in the previous sections. (a) No error. (b) Error on the first qubit. (c) Error on the second qubit. (d) Error on the third qubit.

toolbox [29]. The three qubits are initiated with an Ising coupling of  $J^z/(2\pi) = 40$  MHz between them. The two first qubits are initiated in the state  $|0\rangle$ , while the third qubit is initiated in the normalized state

$$|\psi\rangle = \alpha|0\rangle + \beta|1\rangle. \quad (14)$$

The system is then operated as a  $C(\text{NOT})^2$  gate by driving the two first qubits with an amplitude of  $J = J^z/5$  for the time  $T = \pi/J$ . After this a bit-flip error might occur. This is followed by another driving of the two first qubits for  $T = \pi/J$ . Finally the last qubit is driven for one period. All this is done in less than 200 ns. By averaging over the Bloch sphere for the input state  $|\psi\rangle$  in Eq. (14) we find the average fidelity of the code. In Fig. 5 we present the average fidelities for the three-qubit error correction code for a single bit-flip on the different bits. From the simulation we see that the error is corrected with a fidelity above 0.99.

## B. Steane code

The Steane code is a bit more intricate than the three-qubit as it involves encoding on seven qubits. This is two more than the minimum number of qubits needed for protection against both bit flip and phase errors [2], however it is the simplest CSS code which protects against both bit flip and phase errors. The encoding scheme for the Steane code can be seen in Fig. 6.

As the encoding scheme only uses  $C(\text{NOT})^2$  and  $C(\text{NOT})^3$  gates, it is necessary to be able to perform gate operations on some of the seven qubit but not all. This can be achieved *in situ* in superconducting circuits by varying the magnetic flux through the Josephson junctions which connects qubits which are desired unconnected. An overview on how to connect the seven qubits in the four steps of the encoding can be seen in Fig. 7. Using the

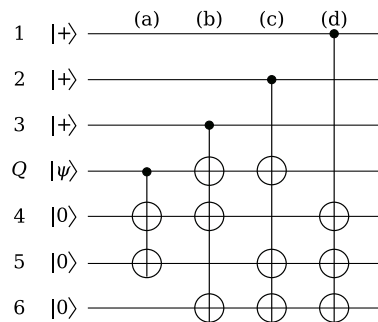


Figure 6. Encoding scheme for the Steane code. The state of qubit  $Q$ ,  $|\psi\rangle$  is encoded into the seven-qubit, using one  $C(\text{NOT})^2$  gate and three  $C(\text{NOT})^3$  gates. The first three qubits are prepared in the state  $|+\rangle = (|0\rangle + |1\rangle)/\sqrt{2}$ , while the last three qubits are prepared in the state  $|0\rangle$ .

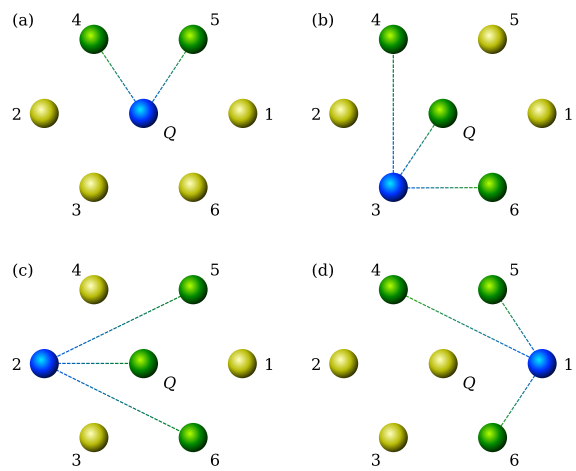


Figure 7. The four steps realizing the Steane code using  $C(\text{NOT})^n$  gates. Green spheres represent target qubit, i.e., qubits which the NOT-operation is performed on, blue spheres are control qubits, and the yellow spheres represents idle qubits. The four steps (a)-(d) corresponds to the four gates in Fig. 6.

regular CNOT-gate the Steane encoding takes 11 steps, while with  $C(\text{NOT})^n$ -gates it can be done in just four steps.

We simulate the system using the Lindblad Master equation. Seven qubits are initiated, three in the state  $|+\rangle = (|0\rangle + |1\rangle)/\sqrt{2}$ , three in the state  $|0\rangle$ , while the last qubit is initiated in the state of Eq. (14). The Ising coupling is in all cases  $J^z/(2\pi) = 40$  MHz, and the driving of the target qubits is the same for all steps, yielding a total time of  $4T$  for the encoding to be implemented. We average over the Bloch sphere for the input state  $|\psi\rangle$  in order to find the average fidelity. The fidelity is found by taking the overlap between the seven-qubit output state and the state  $\alpha|0\rangle_L + \beta|1\rangle_L$ , where the expression for the two states  $|0\rangle_L$  and  $|1\rangle_L$  is the appropriate encoding states for the Steane code, with the phases of the  $C(\text{NOT})^n$  gates added. These can be seen in Appendix C. These phases are well known and do not influence the encoding.

The results of the simulation can be seen in Fig. 8. The

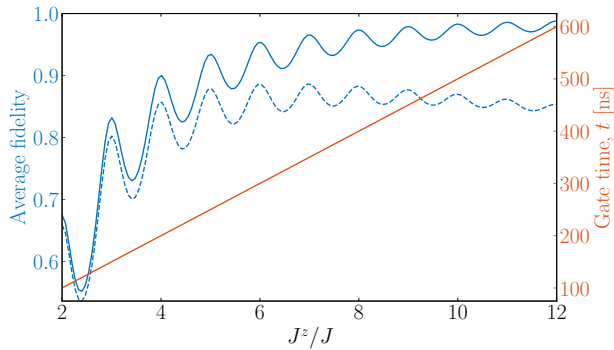


Figure 8. Simulation of the Steane encoding scheme seen in Fig. 6, using  $C(\text{NOT})^n$  gates. The simulation is done for  $J^z/(2\pi) = 40$  MHz. The blue line indicates the average fidelity, while the red line indicates the gate time  $T$ . The dashed blue line is the average fidelity with a decoherence time of  $T_1 = T_2 = 30 \mu\text{s}$ , while the solid is without decoherence.

result is similar to the one presented in Fig. 2, however, with longer gate times and lower fidelities. When not considering decoherence, the lower fidelity is also a result of the fact that we need four gates, and thus the infidelity of each gate accumulate. The fact that the fidelity peaks just below 0.9 when including decoherence in the simulation is due to the fact that seven qubits increases the amount of decoherence. The longer gate time is a result of the fact that we are now dealing with four gates, compared to one in Fig. 2. However, this is still a rather short time compared to if we had only used two-qubit gates, which would increase the gate time by almost a factor of three.

## V. CONCLUSION AND OUTLOOK

We have proposed a simple single-step implementation of  $n$ -bit Toffoli gates and  $C(\text{NOT})^n$ -gates and shown that these exhibit a high fidelity for up to 6 qubits. As an example of a an implementation of the gates for quantum information processing we have included a superconducting circuit design of the gates, though the idea is not limited to superconducting circuits.

By simulating the gates we have shown that the gates can easily be concatenated into error correction codes. The gates proposed in this paper are not limited to the three-qubit error correcting code or the Steane code. They can be applied to numerous other codes making them more effective.

The gates proposed in this paper can easily be transformed into  $C^nZ$  or  $CZ^n$  gates. This can of course be done by applying Hadamard gates to the qubits which are being flipped, however, there is a more elegant way to do this. If we exchange the Pauli  $X$ -operators with  $Z$ -operators in Eq. (1) or Eq. (11) and vica versa we obtain  $C^nZ$  or  $CZ^n$  gates respectively. This is the same idea as applying Hadamard gate before and after, as the Hadamard gates effectively changes the basis.

## ACKNOWLEDGMENTS

The authors would like to thank K. S. Christensen, T. Bækkegaard, L. B. Kristensen, and N. J. S. Loft for discussion on different aspects of the work. This work is supported by the Danish Council for Independent Research and the Carlsberg Foundation.

- 
- [1] T. Toffoli, in *Automata, Languages and Programming*, edited by J. de Bakker and J. van Leeuwen (Springer Berlin Heidelberg, Berlin, Heidelberg, 1980) pp. 632–644.
- [2] M. A. Nielsen and I. L. Chuang, *Quantum Computation and Quantum Information: 10th Anniversary Edition* (Cambridge University Press, 2010).
- [3] D. G. Cory, M. D. Price, W. Maas, E. Knill, R. Laflamme, W. H. Zurek, T. F. Havel, and S. S. Somaroo, *Phys. Rev. Lett.* **81**, 2152 (1998).
- [4] P. Schindler, J. T. Barreiro, T. Monz, V. Nebendahl, D. Nigg, M. Chwalla, M. Hennrich, and R. Blatt, *Science* **332**, 1059 (2011).
- [5] E. Dennis, *Phys. Rev. A* **63**, 052314 (2001).
- [6] A. Paetznick and B. W. Reichardt, *Phys. Rev. Lett.* **111**, 090505 (2013).
- [7] P. W. Shor, *Phys. Rev. A* **52**, R2493 (1995).
- [8] C. Monroe, D. M. Meekhof, B. E. King, W. M. Itano, and D. J. Wineland, *Phys. Rev. Lett.* **75**, 4714 (1995).
- [9] E. Brion, D. Comparat, and G. Harel, *The European Physical Journal D - Atomic, Molecular, Optical and Plasma Physics* **38**, 381 (2006).
- [10] T. Noh, G. Park, S. Lee, W. Song, and Y. Chong, “Construction of controlled-not gate based on microwave-activated phase (map) gate in two transmon system,” (2018), arXiv:1803.04105.
- [11] T. P. Gujarati, *Phys. Rev. A* **98**, 062326 (2018).
- [12] N. Yu, R. Duan, and M. Ying, *Phys. Rev. A* **88**, 010304 (2013).
- [13] A. Barenco, C. H. Bennett, R. Cleve, D. P. DiVincenzo, N. Margolus, P. Shor, T. Sleator, J. A. Smolin, and H. Weinfurter, *Phys. Rev. A* **52**, 3457 (1995).
- [14] T. Monz, K. Kim, W. Hänsel, M. Riebe, A. S. Villar, P. Schindler, M. Chwalla, M. Hennrich, and R. Blatt, *Phys. Rev. Lett.* **102**, 040501 (2009).
- [15] M. Mičuda, M. Sedlák, I. Straka, M. Miková, M. Dušek, M. Ježek, and J. Fiurášek, *Phys. Rev. Lett.* **111**, 160407 (2013).
- [16] A. Fedorov, L. Steffen, M. Baur, M. P. da Silva, and A. Wallraff, *Nature* **481**, 170 EP (2011).
- [17] M. D. Reed, L. DiCarlo, S. E. Nigg, L. Sun, L. Frunzio, S. M. Girvin, and R. J. Schoelkopf, *Nature* **482**, 382 (2012).
- [18] A. M. Chen, S. Y. Cho, and M. D. Kim, *Phys. Rev. A* **85**, 032326 (2012).

- [19] X.-F. Shi, Phys. Rev. Applied **9**, 051001 (2018).
- [20] Y. Cao, G. C. Wang, H. D. Liu, and C. F. Sun, Scientific reports **8**, 5813 (2018), 29643455[pmid].
- [21] B. P. Lanyon, M. Barbieri, M. P. Almeida, T. Jennewein, T. C. Ralph, K. J. Resch, G. J. Pryde, J. L. O’Brien, A. Gilchrist, and A. G. White, Nature Physics **5**, 134 (2008), article.
- [22] I. I. Beterov, I. N. Ashkarin, E. A. Yakshina, D. B. Tretyakov, V. M. Entin, I. I. Ryabtsev, P. Cheinet, P. Pillet, and M. Saffman, Phys. Rev. A **98**, 042704 (2018).
- [23] D. Maslov and G. W. Dueck, Electronics Letters **39**, 1790 (2003).
- [24] Jia-Lin Chen, Xiao-Ying Zhang, Ling-Li Wang, Xin-Yuan Wei, and Wen-Qing Zhao, in *2008 9th International Conference on Solid-State and Integrated-Circuit Technology* (2008) pp. 575–578.
- [25] D. C. McKay, C. J. Wood, S. Sheldon, J. M. Chow, and J. M. Gambetta, Phys. Rev. A **96**, 022330 (2017).
- [26] M. A. Nielsen, Physics Letters A **303**, 249 (2002).
- [27] M. Horodecki, P. Horodecki, and R. Horodecki, Phys. Rev. A **60**, 1888 (1999).
- [28] B. Schumacher, Phys. Rev. A **54**, 2614 (1996).
- [29] J. Johansson, P. Nation, and F. Nori, Computer Physics Communications **183**, 1760 (2012).
- [30] G. Wendin, Reports on Progress in Physics **80**, 106001 (2017).
- [31] K. S. Christensen, S. E. Rasmussen, D. Petrosyan, and N. T. Zinner, “A coherent router for quantum networks,” (2019), arXiv:1909.11412.
- [32] J. Koch, T. M. Yu, J. Gambetta, A. A. Houck, D. I. Schuster, J. Majer, A. Blais, M. H. Devoret, S. M. Girvin, and R. J. Schoelkopf, Phys. Rev. A **76**, 042319 (2007).
- [33] J. A. Schreier, A. A. Houck, J. Koch, D. I. Schuster, B. R. Johnson, J. M. Chow, J. M. Gambetta, J. Majer, L. Frunzio, M. H. Devoret, S. M. Girvin, and R. J. Schoelkopf, Phys. Rev. B **77**, 180502 (2008).
- [34] M. Kounalakis, C. Dickel, A. Bruno, N. K. Langford, and G. A. Steele, npj Quantum Information **4**, 38 (2018).
- [35] A. M. Steane, Proc. R. Soc. Lond. A. **452**, 2551–2577 (1996).
- [36] A. M. Steane, Phys. Rev. Lett. **77**, 793 (1996).
- [37] A. A. Houck, J. Koch, M. H. Devoret, S. M. Girvin, and R. J. Schoelkopf, Quantum Information Processing **8**, 105 (2009).
- [38] J. Chiaverini, D. Leibfried, T. Schaetz, M. D. Barrett, R. B. Blakestad, J. Britton, W. M. Itano, J. D. Jost, E. Knill, C. Langer, R. Ozeri, and D. J. Wineland, Nature **432**, 602 (2004).
- [39] D. Nigg, M. Müller, E. A. Martinez, P. Schindler, M. Hennrich, T. Monz, M. A. Martin-Delgado, and R. Blatt, Science **345**, 302 (2014).
- [40] M. H. Devoret, in *Fluctuations Quantiques/Quantum Fluctuations: Les Houches Session LXIII*, edited by S. Reynaud, E. Giacobino, and J. Zinn-Justin (Elsevier, 1997) p. 351.
- [41] U. Vool and M. H. Devoret, International Journal of Circuit Theory and Applications **45**, 897 (2017).
- [42] W. S. Warren, The Journal of Chemical Physics **81**, 5437 (1984).
- [43] M. Steffen, J. M. Martinis, and I. L. Chuang, Phys. Rev. B **68**, 224518 (2003).
- [44] P. Rebentrost and F. K. Wilhelm, Phys. Rev. B **79**, 060507 (2009).
- [45] F. Motzoi, J. M. Gambetta, P. Rebentrost, and F. K. Wilhelm, Phys. Rev. Lett. **103**, 110501 (2009).
- [46] J. M. Gambetta, F. Motzoi, S. T. Merkel, and F. K. Wilhelm, Phys. Rev. A **83**, 012308 (2011).
- [47] P. de Fouquieres, S. Schirmer, S. Glaser, and I. Kuprov, Journal of Magnetic Resonance **212**, 412 (2011).
- [48] F. Motzoi and F. K. Wilhelm, Phys. Rev. A **88**, 062318 (2013).

### Appendix A: Analysis of the superconducting circuit

Following the procedure of Refs. [40, 41] we obtain the following Lagrangian from the circuit diagram in Fig. 1(b)

$$L = 2 \sum_{i=0}^n C_i \dot{\varphi}_i^2 + 2 \sum_{i=1}^n C_{z,i} (\dot{\varphi}_i - \dot{\varphi}_0)^2 + \sum_{i=0}^n E_i \cos \varphi_i + \sum_{i=1}^n E_{z,i} \cos(\varphi_0 - \varphi_i), \quad (\text{A1})$$

where  $\hat{\varphi}_i$  are the node fluxes across the Josephson junctions of the respective qubits. The two first terms come from the capacitors and are interpreted as kinetic terms, and the remaining terms come from the Josephson junctions and are interpreted as potential terms. The  $n$  indicates the number of blue transmon qubits on the circuit diagram, i.e., in Fig. 1(b)  $n = 2$ .

The Lagrangian can be rewritten into the Hamiltonian in Eq. (10) doing the usual Legendre transformation. The capacitance matrix in the 2-bit case is then

$$K = \begin{bmatrix} C_0 + C_{z,1} + C_{z,2} & -C_{z,1} & -C_{z,2} \\ -C_{z,1} & C_1 + C_{z,1} & 0 \\ -C_{z,2} & 0 & C_2 + C_{z,2} \end{bmatrix}. \quad (\text{A2})$$

while in the 3-bit case (see Fig. 9 for circuit diagram of the 3-bit case) it becomes

$$K = \begin{bmatrix} C_0 + C_{z,1} + C_{z,2} + C_{z,3} & -C_{z,1} & -C_{z,2} & -C_{z,3} \\ -C_{z,1} & C_1 + C_{z,1} & 0 & 0 \\ -C_{z,2} & 0 & C_2 + C_{z,2} & 0 \\ -C_{z,3} & 0 & 0 & C_3 + C_{z,3} \end{bmatrix}, \quad (\text{A3})$$

and so on for higher  $n$ . The typical transmon have a charging energy much smaller than the junction energy, and therefore the phase is well localized near the bottom of the potential. We can therefore expand the potential part of the Hamiltonian to fourth order

$$\begin{aligned} U(\varphi) &= \sum_{i=0}^n E_i \left[ \frac{1}{2} \varphi_i^2 - \frac{1}{24} \varphi_i^4 \right] + \sum_{i=1}^n E_{z,i} \left[ \frac{1}{2} (\varphi_i - \varphi_0)^2 - \frac{1}{24} (\varphi_i - \varphi_0)^4 \right] \\ &= \sum_{i=0}^n E_i \left[ \frac{1}{2} \varphi_i^2 - \frac{1}{24} \varphi_i^4 \right] + \sum_{i=1}^n E_{z,i} \left[ \frac{1}{2} (\varphi_i^2 + \varphi_0^2 - 2\varphi_i \varphi_0) - \frac{1}{24} (\varphi_i^4 + \varphi_0^4 - 4\varphi_i^3 \varphi_0 + 6\varphi_i^2 \varphi_0^2 - 4\varphi_i \varphi_0^3) \right]. \end{aligned}$$

By collecting terms we can write the full Hamiltonian as

$$\begin{aligned} H &= \sum_{i=0}^n \left[ \frac{1}{2} E_i^C p_i^2 + \frac{1}{2} E_i^J \varphi_i^2 - \frac{1}{24} E_i^J \varphi_i^4 \right] + \sum_{i=1}^n (K^{-1})_{(i,0)} p_i p_0 \\ &\quad + \sum_{i>j=1}^n (K^{-1})_{(i,j)} p_i p_j + \sum_{i=1}^n E_{z,i} \left[ -\frac{1}{4} \varphi_i^2 \varphi_0^2 - \varphi_i \varphi_0 + \frac{1}{6} (\varphi_i^3 \varphi_0 + \varphi_i \varphi_0^3) \right], \end{aligned}$$

where the effective energy of the capacitances is  $E_i^C = (K^{-1})_{(i,i)}/8$ . Note that there is a capacitive coupling between all of the qubits regardless of whether there actually is a capacitor between them. The effective Josephson energies are

$$E_i^J = E_i + E_{z,i} \quad \text{for } i \neq 0, \quad (\text{A4a})$$

$$E_0^J = E_0 + \sum_{i=1}^n E_{z,i}. \quad (\text{A4b})$$

We now do the canonical quantization  $\varphi_i \rightarrow \hat{\varphi}_i$  and  $p_i \rightarrow \hat{p}_i$ , requiring that  $[\hat{p}_i, \hat{\varphi}_j] = i\delta_{ij}$ . This allows us to change into ladder operators

$$\hat{\varphi}_i = \sqrt{\frac{\zeta_i}{2}} (\hat{b}_i^\dagger + \hat{b}_i), \quad \hat{p}_i = \frac{i}{\sqrt{2\zeta_i}} (\hat{b}_i^\dagger - \hat{b}_i), \quad (\text{A5})$$

with impedance  $\zeta_i = \sqrt{(K^{-1})_{(i,i)}/E_i^J}$ , and the Hamiltonian takes the form

$$\begin{aligned} \hat{H} &= \sum_{i=0}^n \left[ \sqrt{8E_i^C E_i^J} \hat{b}_i^\dagger \hat{b}_i - \frac{E_i^C}{12} (\hat{b}_i^\dagger + \hat{b}_i)^4 \right] - \frac{1}{2} \sum_{i=1}^n \frac{(K^{-1})_{(i,0)}}{\sqrt{\zeta_i \zeta_0}} (\hat{b}_i^\dagger - \hat{b}_i) (\hat{b}_0^\dagger - \hat{b}_0) \\ &\quad - \frac{1}{2} \sum_{i>j=1}^n \frac{(K^{-1})_{(i,j)}}{\sqrt{\zeta_i \zeta_j}} (\hat{b}_i^\dagger - \hat{b}_i) (\hat{b}_j^\dagger - \hat{b}_j) \\ &\quad + \sum_{i=1}^n E_{z,i} \left[ -\frac{1}{24} \zeta_i \zeta_0 (\hat{b}_i^\dagger + \hat{b}_i)^2 (\hat{b}_0^\dagger + \hat{b}_0)^2 - \frac{1}{2} \sqrt{\zeta_i \zeta_0} (\hat{b}_i^\dagger + \hat{b}_i) (\hat{b}_0^\dagger + \hat{b}_0) \right. \\ &\quad \left. + \frac{1}{24} \left( \zeta_i \sqrt{\zeta_i \zeta_0} (\hat{b}_i^\dagger + \hat{b}_i)^3 (\hat{b}_0^\dagger + \hat{b}_0) + \zeta_0 \sqrt{\zeta_i \zeta_0} (\hat{b}_i^\dagger + \hat{b}_i) (\hat{b}_0^\dagger + \hat{b}_0)^3 \right) \right]. \end{aligned}$$

If the anharmonicity,  $\alpha_i = E_i^C/2$ , of the qubits are sufficiently large, we can justify projecting the Hamiltonian into the lowest two eigenstates of each qubit

$$\hat{H} = -\frac{1}{2} \sum_{i=0}^n \Omega_i \sigma_i^z + \frac{1}{2} \sum_{n=1}^n J_n^z \sigma_n^z \sigma_0^z + \frac{1}{2} \sum_{i=1}^n J_i^x (\sigma_i^+ \sigma_0^- + \sigma_i^- \sigma_0^+) + \frac{1}{2} \sum_{i \neq j=1}^n J_{ij}^x (\sigma_i^+ \sigma_j^- + \sigma_i^- \sigma_j^+), \quad (\text{A6})$$

where we have neglected terms that do not conserve number excitation, such as  $\sigma_i^\pm \sigma_j^\pm$  (this is the rotating wave approximation). We note that the first term is the desired non-interacting Hamiltonian, and the second term is the

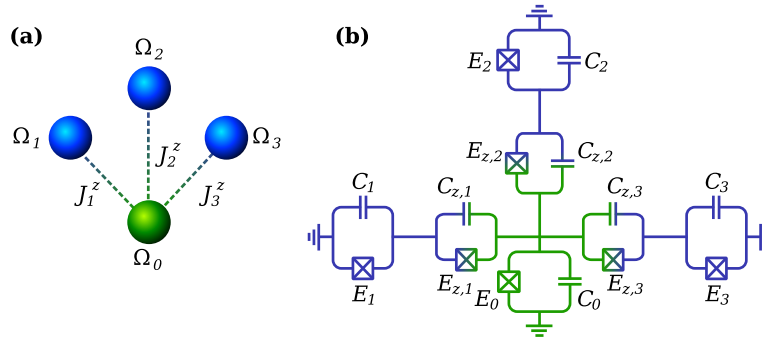


Figure 9. Implementation of the 3-bit Toffoli gate. Figure (a) shows a schematic representation of the model implementing the 3-bit Toffoli gate, with the green sphere representing the target qubit and the blue spheres representing the control qubits. Figure (b) shows the superconducting circuit yielding the model in figure (a). The different parts of the system are colored according to their role, as per (a).

desired Ising coupling term. The qubit frequencies and the coupling strengths are given as

$$\Omega_i = \sqrt{8E_i^C E_i^J} + \frac{1}{2}E_i^C + \frac{1}{6}E_{z,i}\zeta_i\zeta_0 \quad \text{for } i \neq 0, \quad (\text{A7a})$$

$$\Omega_0 = \sqrt{8E_0^C E_0^J} + \frac{1}{2}E_0^C + \frac{1}{6} \sum_{i=1}^n E_{z,i}\zeta_i\zeta_0, \quad (\text{A7b})$$

$$J_i^z = -\frac{1}{12}E_{z,i}\zeta_i\zeta_0, \quad (\text{A7c})$$

$$J_i^x = \frac{(K^{-1})_{(i,0)}}{\sqrt{\zeta_i\zeta_0}} - E_i\sqrt{\zeta_i\zeta_0} + \frac{1}{4}E_i(\zeta_i + \zeta_0)\sqrt{\zeta_i\zeta_0}, \quad (\text{A7d})$$

$$J_{ij}^x = \frac{(K^{-1})_{(i,j)}}{\sqrt{\zeta_i\zeta_j}}. \quad (\text{A7e})$$

If the detunings  $\Delta_{i0} = \Omega_i - \Omega_0$ , of the zeroth qubit compared to all other qubits are all much larger than the transverse couplings in Eq. (A7d), we can ignore the first order excitation swaps between these qubits. In this case the Hamiltonian takes the form

$$\hat{H} = \hat{H}_0 + \frac{1}{2} \sum_{n=1}^n J_n^z \sigma_n^z \sigma_0^z + \frac{1}{2} \sum_{i \neq j=1}^n J_{ij}^x (\sigma_i^+ \sigma_j^- + \sigma_i^- \sigma_j^+). \quad (\text{A8})$$

The last term represents the cross couplings between the  $i$ th and  $j$ th qubit for  $i, j = 1, 2, \dots, n$ . We can get rid of this term by requiring  $C_{z,i} \ll C_i$ , which make the Hamiltonian take the desired form.

### 1. The driving term

We are now ready to consider the driving term, i.e., the last term of Eq. (1). If we drive the system capacitively, which yields the following driving Lagrangian

$$L_d = \frac{C_d}{2} (\dot{\phi}_i - \dot{\phi}_i)^2, \quad (\text{A9})$$

which drives the  $i$ th qubit. We simply add such terms for each qubit we wish to drive. The external driving field is given as

$$\phi_i = A \sin(\tilde{\omega}_i t + \theta), \quad (\text{A10})$$

where  $A$  is the amplitude of the driving,  $\tilde{\omega}_i$  is the driving frequency, and  $\theta$  the phase. We rewrite the driving terms as

$$\phi_i = A (\cos \theta \sin \tilde{\omega}_i t + \sin \theta \cos \tilde{\omega}_i t),$$

where we have expanded the driving field in the in-phase component and the out-of-phase component. Expanding the parenthesis of  $L_d$  yields

$$L_d = \frac{C_d}{2} \left[ \dot{\varphi}_i^2 + \dot{\phi}_i^2 - 2\dot{\varphi}_i\dot{\phi}_i \right], \quad (\text{A11})$$

where the first term is a kinetic term which can be absorbed into the diagonal of the capacitance matrix, the second term is some irrelevant offset term, while the last term is the interesting term regarding the driving of the system. This alters the conjugate momentum slightly

$$\mathbf{p} = K\dot{\boldsymbol{\varphi}} + \dot{\boldsymbol{\phi}}, \quad (\text{A12})$$

where  $\boldsymbol{\varphi}$  is the vector of node fluxes, and  $\boldsymbol{\phi}$  is the vector of driving terms. Doing a Legendre transformation the kinetic part of the Hamiltonian takes the form

$$\begin{aligned} H_{\text{kin}} &= 4(\mathbf{p} - \dot{\boldsymbol{\phi}})^T K^{-1} (\mathbf{p} - \dot{\boldsymbol{\phi}}) \\ &= 4 \left[ \mathbf{p}^T K^{-1} \mathbf{p} + \dot{\boldsymbol{\phi}}^T K^{-1} \dot{\boldsymbol{\phi}} - \mathbf{p}^T K^{-1} \dot{\boldsymbol{\phi}} - \dot{\boldsymbol{\phi}}^T K^{-1} \mathbf{p} \right]. \end{aligned}$$

The first term is the original kinetic term (with the added driving capacitance), the second term is the irrelevant offset term, and the last two terms are the driving terms yielding

$$H_d = -\dot{\phi}_i (K^{-1})_{(i,i)} p_i. \quad (\text{A13})$$

Doing the canonical quantization and changing into step operators we obtain

$$\hat{H}_d = -i\dot{\phi}_i \frac{(K^{-1})_{(i,i)}}{\sqrt{2\zeta_i}} \left( \hat{b}_i^\dagger - \hat{b}_i \right), \quad (\text{A14})$$

Truncating to a two-level model as above we find

$$\hat{H}_d = -\dot{\phi}_i \frac{(K^{-1})_{(i,i)}}{\sqrt{2\zeta_i}} \sigma_i^y, \quad (\text{A15})$$

from which we realize that

$$B_i(t) = -A\tilde{\omega}_i \frac{(K^{-1})_{(i,i)}}{\sqrt{2\zeta_i}} (\cos \theta \cos \tilde{\omega}_i t - \sin \theta \sin \tilde{\omega}_i t), \quad (\text{A16})$$

and if we chose  $\theta = 0$  and  $\tilde{\omega}_i = \Omega_i + \omega_i$  we see that  $J = -A(\Omega_i + \omega_i)(K^{-1})_{(i,i)}/\sqrt{2\zeta_i}$ . Note that we need not necessarily  $\theta = 0$  for the gate to work. In fact it can be an advantage to have an out-of-phase component in order to minimize leakage to higher excited states, when the anharmonicity is small using e.g. pulse-shape engineering schemes [42–48].

## Appendix B: Realistic parameters

Here we presents parameters for the circuit model in Fig. 1(b) which yields the desired gate model of Fig. 1(c). The parameters are found by calculating the gate model parameters in Eq. (A7) and then minimizing a cost function which returns a low value when the requirements of the gate model is met. In order to judge the quality of the circuit parameters we also calculate the relative anharmonicity of the 2-level systems, i.e., the difference between the 01 and the 12 transition, and the ratio between the effective Josephson energy and the effective capacitive energy.

In order to simplify the numerical investigation we have assumed that the parameters of the control qubits are identical. The parameters obtained are presented in Table I. As expected we see that the capacitance of the coupling  $C_{z,i}$  should be low compared to the other couplings. We note that we get Ising couplings in the range  $|J^z| \in [25, 320]$  and in all cases dominating the cross coupling  $J_{ij}^x$ . The swapping couplings  $J_i^x$  are all several factors lower than the detunings  $\Delta_{i0} = |\Omega_i - \Omega_0|$

We simulate all of the gates in Table I and find that all result in a maximum fidelity above 0.99, when the driving is  $J = J_i^z/5$ . The average fidelity as a function of time can be seen in Fig. 10.

Table I. Circuit and corresponding gate model parameters for possible Toffoli gates. Since the circuit parameter space is rather large we have several possible solutions, some, but far from all, possible solutions are show in the table. The different solutions are labeled and color coded in the first column. The colorcoding corresponds to the simulation results seen in Fig. 10. The second column shows the circuit parameters for the circuit in Fig. 1(b).  $E_0$ ,  $E_i$ , and  $E_{z,i}$  indicates the Josephson junction of the target qubit, the control qubits and the coupling between them, respectively.  $C_0$ ,  $C_i$ , and  $C_{z,i}$  indicates the capacitance of the target qubit, the control qubits and the coupling between them, respectively. The second column shows the obtained gate parameters, which can be seen in Eq. (A7). The last column show the quality parameters of the gate.  $\alpha_0$  and  $\alpha_i$  are the anharmonicities of the target and control qubits, respectively, while  $E_0^J/E_0^C$  and  $E_i^J/E_i^C$  are the ratios between the effective Josephson energy and effective capacitive energy. The subscript  $i$  indicates  $i = 1, 2$ , i.e., the control qubits.

#	Circuit parameters						Gate parameters					Quality parameters			
	$E_0$ [2 $\pi$ GHz]	$E_i$ [2 $\pi$ GHz]	$E_{z,i}$ [2 $\pi$ GHz]	$C_0$ [fF]	$C_i$ [fF]	$C_{z,i}$ [fF]	$\Omega_0$ [2 $\pi$ GHz]	$\Omega_i$ [2 $\pi$ GHz]	$J_i^z$ [2 $\pi$ MHz]	$J_i^x$ [2 $\pi$ MHz]	$J_{ij}^x$ [2 $\pi$ MHz]	$\alpha_0$ [%]	$\alpha_i$ [%]	$E_0^J/E_0^C$	$E_i^J/E_i^C$
1	20.05	1.26	33.28	15.83	37.84	0.04	30.9	12.8	-320.1	452.6	27.8	-2.0	-2.0	71.1	67.5
2	0.61	0.02	29.30	22.19	44.89	0.03	21.9	10.8	-287.2	5.7	14.9	-2.0	-2.0	68.0	68.0
3	33.65	1.27	28.70	15.37	43.40	0.03	32.0	11.1	-274.0	453.3	22.5	-2.0	-2.0	72.6	67.2
4	31.29	0.71	24.10	16.96	53.10	0.03	28.4	9.2	-233.0	254.9	16.7	-2.0	-2.0	69.9	68.0
5	4.95	1.20	21.94	27.06	57.03	0.05	17.9	8.5	-214.0	433.7	15.0	-2.0	-2.0	68.5	68.2
6	1.58	1.27	17.14	41.71	56.41	0.09	12.5	7.6	-177.1	474.8	14.6	-1.9	-2.2	77.5	53.7
7	39.72	0.11	18.27	17.83	71.69	0.03	26.9	6.8	-176.0	38.3	9.8	-2.0	-2.0	70.4	68.0
8	0.56	0.03	17.53	35.36	77.67	0.08	13.4	6.4	-172.2	12.4	13.1	-2.0	-2.0	65.3	70.5
9	45.01	1.22	16.13	17.72	76.22	0.02	27.1	6.4	-154.6	437.1	7.8	-2.0	-2.0	70.9	68.3
10	19.87	1.22	11.35	31.88	105.46	0.04	15.1	4.6	-109.1	437.3	4.8	-2.0	-2.0	70.2	68.4
11	57.40	1.25	7.45	19.24	153.26	0.01	24.9	3.2	-70.6	444.1	1.7	-2.0	-2.0	71.9	68.8
12	23.81	0.80	6.30	37.75	187.62	0.02	12.7	2.6	-60.1	287.2	1.0	-2.0	-2.0	71.0	68.9
13	58.41	0.09	3.85	21.01	338.06	0.00	22.7	1.4	-36.6	31.3	0.0	-2.0	-2.0	71.7	68.7
14	0.01	0.19	2.50	299.11	386.88	0.37	1.7	1.1	-25.8	71.1	1.3	-1.9	-2.2	77.5	53.7

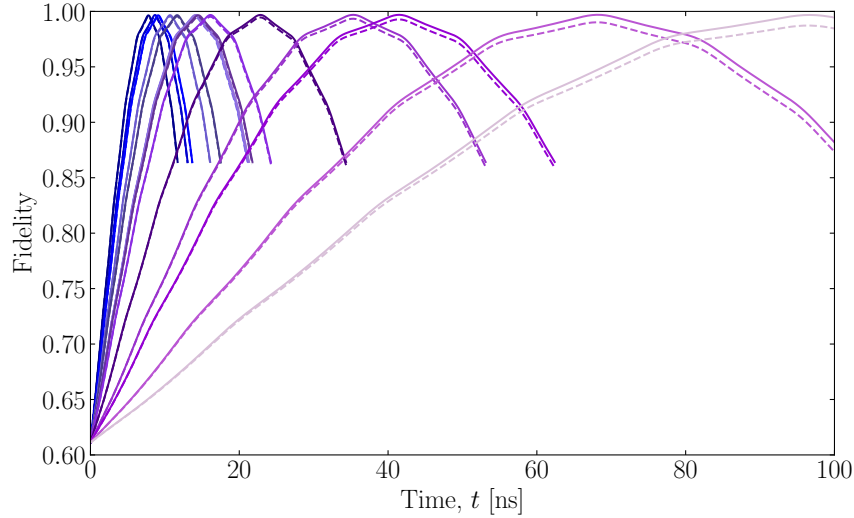


Figure 10. Average fidelity as a function of time for all the gate configurations presented in Table I. All simulations are done for at driving of  $J = J^z/5$ . The solid lines are simulations without decoherence, while the dashed line includes decoherence. The color of the line corresponds to the colors in Table I.

### Appendix C: Steane encoding states

We derive the two Steane encoding states  $|0\rangle_L$  and  $|1\rangle_L$ , by applying the  $C(\text{NOT})^n$  gates to the initial states

$$\begin{aligned}
|+++0000\rangle &= \frac{1}{2\sqrt{2}}(|0\rangle + |1\rangle)(|0\rangle + |1\rangle)(|0\rangle + |1\rangle)|0000\rangle \\
&\xrightarrow{C(\text{NOT})^2} \frac{1}{2\sqrt{2}}(|0\rangle + |1\rangle)(|0\rangle + |1\rangle)(|0\rangle + |1\rangle)|0000\rangle \\
&\xrightarrow{C(\text{NOT})^3} \frac{1}{2\sqrt{2}}(|0\rangle + |1\rangle)(|0\rangle + |1\rangle)(|00000\rangle + i|11101\rangle) \\
&\xrightarrow{C(\text{NOT})^3} \frac{1}{2\sqrt{2}}(|0\rangle + |1\rangle)(|000000\rangle + i|101011\rangle + i(|011101\rangle + i|110110\rangle)) \\
&\xrightarrow{C(\text{NOT})^3} |0\rangle_L = \frac{1}{2\sqrt{2}}(|0000000\rangle + i|0101011\rangle + i|0011101\rangle - |0110110\rangle \\
&\quad + i|1000111\rangle - |1101100\rangle - |1011010\rangle - i|1110001\rangle),
\end{aligned}$$

$$\begin{aligned}
|+++1000\rangle &= \frac{1}{2\sqrt{2}}(|0\rangle + |1\rangle)(|0\rangle + |1\rangle)(|0\rangle + |1\rangle)|1000\rangle \\
&\xrightarrow{C(\text{NOT})^2} \frac{1}{2\sqrt{2}}(|0\rangle + |1\rangle)(|0\rangle + |1\rangle)(|0\rangle + |1\rangle)|1110\rangle \\
&\xrightarrow{C(\text{NOT})^3} \frac{1}{2\sqrt{2}}(|0\rangle + |1\rangle)(|0\rangle + |1\rangle)(|01110\rangle + i|10011\rangle) \\
&\xrightarrow{C(\text{NOT})^3} \frac{1}{2\sqrt{2}}(|0\rangle + |1\rangle)(|001110\rangle + i|010011\rangle + i(|100101\rangle + i|111000\rangle)) \\
&\xrightarrow{C(\text{NOT})^3} |1\rangle_L = \frac{1}{2\sqrt{2}}(-|0001110\rangle - i|0010011\rangle - i|0100101\rangle + |0111000\rangle \\
&\quad - i|1001001\rangle + |1100010\rangle + |1010100\rangle + i|1111111\rangle).
\end{aligned}$$